

### Dalton Transactions

## UV-Vis spectrophotometric determination of rare earth elements (REE) speciation at near-neutral to alkaline pH. Part I: m-cresol purple properties from 25-75 °C and Er hydrolysis

Journal:	Dalton Transactions	
Manuscript ID	DT-ART-05-2024-001515.R3	
Article Type:	Paper	
Date Submitted by the Author:	13-Jul-2024	
Complete List of Authors:	Han, Hannah Juan; New Mexico Institute of Mining and Technology, New Mexico Bureau of Geology and Mining Resources Gysi, Alexander; New Mexico Institute of Mining and Technology, Earth and Environmental Science; New Mexico Bureau of Geology & Mineral Resources, New Mexico Institute of Mining and Technology	

SCHOLARONE™ Manuscripts

# UV-Vis spectrophotometric determination of rare earth elements (REE) speciation at near-neutral to alkaline pH. Part I: m-cresol purple properties from 25-75 °C and Er hydrolysis

Hannah Juan Han\*a, Alexander Gysia,b

<sup>a</sup>New Mexico Bureau of Geology and Mineral Resources, New Mexico Institute of Mining and

Technology, 801 Leroy Place, Socorro, NM 87801, USA

<sup>b</sup>Department of Earth and Environmental Science, New Mexico Institute of Mining and Technology,

801 Leroy Place, Socorro, NM 87801, USA

\* Corresponding authors: hannah.juan.han@nmt.edu

KEYWORDS: Hydrolysis, erbium, rare earth elements; UV-Vis spectrophotometry, meta-cresol purple, pH measurement

#### **Abstract**

The speciation and mobility of rare earth elements (REE) strongly depends on pH which controls the formation of charged aqueous hydroxyl species. The latter potentially play an important role in controlling heavy REE adsorption on clay minerals in near-neutral to alkaline waters such as in regolith-hosted REE mineral deposits. However, accurate REE hydrolysis constants are needed for developing geochemical models that can predict the role of these charged species in natural systems. Here, we develop a robust experimental UV-Vis spectrophotometric method using m-cresol purple to determine in situ pH from 25 to 75 °C. This method is used to derive the average ligand number and hydrolysis constants of erbium (Er) at 25 °C in aqueous solutions with low ionic strength (≤ 0.001 mol/L) at pH from ~7 to 9.5 and in the presence of Er concentrations from 0 to 0.057 mM. The average ligand number ranges between 1 and 3 indicating that Er(OH)<sup>2+</sup>, Er(OH)<sup>2+</sup> and Er(OH)<sup>3</sup> control speciation in the experiments. The logarithm of the Er hydrolysis constants ( $\log^*\beta_n^{\circ}$ , n=1 to 3) derived at infinite dilution for the reaction  $Er^{3+} + nH_2O = Er(OH)_n^{3-n} + nH^+$  are:  $*\beta_1^{\circ} = -7.22 \pm 0.10$ ,  $*\beta_2^{\circ} = -14.52 \pm 0.08$ ,  $*\beta_3^{\circ} = -23.24 \pm 0.04$ . Implementation of these experimental data into a geochemical model indicates that the Er(OH)<sub>2</sub><sup>+</sup> and Er(OH)<sub>3</sub><sup>0</sup> species are both stable in a much wider pH range than previously predicted. Consequently, the positively charged REE hydroxyl complexes can potentially control the fractionation of light vs. heavy REE via adsorption as observed in the formation of certain regolith-hosted REE deposits.

#### 1. Introduction

The rare earth elements (REE) have important applications in the high-tech and green technology industries because of their magnetic, optical, and catalytic properties <sup>1–5</sup>. The increased demand for REE has also resulted in an interest in their behavior in natural systems. The speciation of REE in low temperature aqueous solutions is of particular interest for understanding the fractionation of light versus heavy REE associated to the formation of regolith-hosted ion adsorption deposits <sup>6–8</sup>. Other potential applications include the development of new chemical separation technologies. However, robust experimental techniques are needed to derive accurate thermodynamic data for modeling the mobility of REE and the stability of aqueous complexes as a function of pH.

The recent review by Jordan et al. for the thermodynamic properties of Eu hydroxyl complexes indicates that for some REE, such as Eu, an extensive set of experimental data are available to derive reliable thermodynamic properties <sup>9</sup>. However, experimental speciation data for most of the other REE are limited and many recent REE speciation studies <sup>10,11</sup> still have to rely on thermodynamic data for the hydrolysis of REE compiled by Baes and Mesmer several decades ago <sup>12</sup>. Experimental techniques have improved considerably since then, with reliable potentiometric measurements and UV-Vis spectrophotometry further developed for the study of REE hydrolysis <sup>13–15</sup>. The combination of UV-Vis spectrophotometry with the color indicator *m*-cresol purple (mCP) is a promising method for *in situ* pH measurement and has many practical advantages including ease of use, accessibility to many laboratories, and high sensitivity and selectivity inherent to the color indicator. The combined UV-Vis/mCP method allows conducting experiments at near-neutral to alkaline pH with relatively low REE concentrations and with short equilibration times <sup>13,15</sup>, and has provided reliable pH measurements in natural waters <sup>16–18</sup>.

The combined UV-Vis/mCP method highly depends on the quality of optical properties and dissociation constants derived for mCP. Previous work on the properties of mCP was experimentally conducted at temperatures from −6 to 35 °C at high ionic strength (≥ 0.7 mol/kg) in a number of studies <sup>16,19–23</sup>, and from 8 to 30 °C at relatively low ionic strength (≤ 0.01 mol/L) in the study by Lai et al. <sup>18</sup>. Klungness and Byrne <sup>13</sup> and Stepanchikova et al. <sup>15</sup> have performed UV-Vis experiments at 25 °C to derive the hydrolysis constant for all of the REE at 0.7 and ≤ 0.001 mol/L ionic strengths, respectively. In their studies, mCP dissociation constant were used from Clayton and Byrne <sup>19</sup>, in which the mCP dissociation constant at 0.7 mol/L ionic strength was determined using the pH values for tris buffer reported by Dickson <sup>24</sup> based on the measurements of Ramette et al. <sup>25</sup>. However, DelValls and Dickson later demonstrated that the pH value of the tris buffer solution by Dickson <sup>24</sup> was characterized incorrectly <sup>26</sup>. Therefore, there is a need to develop a robust UV-Vis method for reliable determination of the REE hydrolysis constants in a broad pH and temperature range, and to revise previous thermodynamic data even at 25 °C.

In this study, UV-Vis spectrophotometric experiments were conducted from 25 to 75 °C and at near-neutral to alkaline pH to determine the optical properties and dissociation constants of mCP. Building on the studies by Klungness and Byrne <sup>13</sup> and Stepanchikova et al. <sup>15</sup>, we develop a systematic combined UV-Vis/mCP method for *in situ* pH determination at near-neutral to alkaline pH and retrieve the hydrolysis constants of erbium (Er) at 25 °C. The revised hydrolysis constants are compared with previously reported experimental data and implemented into a geochemical model to determine how the speciation of REE hydroxyl complexes potentially controls the formation of regolith-hosted ion adsorption REE deposits.

**Dalton Transactions** 

#### 2. Methods

#### 2.1. Analytical methods

An Agilent Cary 5000 dual-beam UV-Vis spectrophotometer was used to measure the absorption spectra of mCP from 350 to 750 nm wavelengths. The wavelength accuracy of the instrument was calibrated and verified using the alpha (656.1 nm) and beta (486 nm) emission lines of the deuterium lamp. The spectral bandwidth of the instrument is 2.0 nm. The experimental solutions were loaded in 10 mm path length rectangular quartz cells sealed with Teflon and the temperature was maintained constant using an Agilent dual-cell Peltier temperature control accessory mounted in the UV-Vis instrument. Temperature was recorded using a Cary temperature probe with an accuracy of  $\pm$  0.1 °C. In addition to sealing of the quartz cuvettes, care was taken to minimize any interference with CO<sub>2</sub>(g) in the alkaline solutions by preparing all the experimental solutions daily with CO<sub>2</sub>-degassed and ion exchange column purified Milli-O water.

Potentiometric measurements were carried out in the experimental sample solutions and pH buffer solutions using a Thermo Scientific Orion Star A111 benchtop pH meter and a 9157BNMD Orion Triode combined pH-temperature electrode. The electrode was calibrated at temperatures between 25 and 75 °C using Fisher Scientific commercial buffer solutions with known pH-temperature dependence (pH of 4, 7, and 10 at 25 °C; accuracy of  $\pm$  0.01 pH unit). Both, samples and buffer solutions were submerged in a water bath to keep temperature constant within  $\pm$  0.5 °C.

Erbium concentrations were measured in the experimental and stock solutions using an Agilent 5900 inductively coupled plasma optical emission spectroscopy (ICP-OES) instrument with axial viewing mode. A series of standard Er solutions with concentrations ranging between 20 to 250 ppb were prepared from a 10 ppm Er standard stock solution (Inorganic Ventures, NIST traceable standard) and diluted with a 2 % nitric acid (Fisher Scientific, trace metal grade) blank and Milli-Q water (18.2  $M\Omega$ ·cm). The precision of ICP-OES runs based on repeated 50 ppb standard analysis is better than 3 %; in the concentration range of the Er stock solutions (147 to 176 ppb), the precision

is better than 1.5 %. The limit of detection for Er is 0.8 ppb based on  $5\sigma$  of multiple blank analysis with a limit of quantification of 1.6 ppb based on  $10\sigma$  of the blank.

#### 2.2. Experimental methods

#### 2.2.1. mCP solutions

The optical absorbance properties of mCP were measured using UV-Vis spectrophotometry at temperatures between 25 and 75 °C. A maximum temperature of 75 °C was used in this study due to the challenges (evaporation, leaking, leaching of alkaline solution, etc.) associated with the use of a quartz cell and the application of this study to low temperature geochemical and environmental processes.

The pH buffer solutions were prepared by diluting an aliquot of mCP stock solution with an aliquot of acidic (HCl) or alkaline (NaOH) stock solutions to reach final pH values of 4 or 12. The 0.145 mM mCP stock solution was prepared by dissolving mCP powder (Acros Organics, indicator grade) in Milli-Q water. The 1.0 mM HCl stock solution was prepared by titrating  $0.100 \pm 0.001$  M HCl (Inorganic Ventures, NIST traceable standards) into Milli-Q water to reach a pH of 3. The pH 4 buffer solution was then prepared by diluting a 10.0 g aliquot of 0.145 mM mCP stock solution with 35.0 g of Milli-Q water and 5.0 g of the 1.0 mM HCl acidic stock solution; the pH 12 buffer solution was prepared in a similar way but using  $0.100 \pm 0.001$  M NaOH (Inorganic Ventures, NIST traceable standards) instead of HCl.

The dissociation constants of mCP were determined in fixed pH solutions prepared from a 0.2 M Tris (hydroxymethyl) aminomethane (Tris) buffer solution. The Tris stock solution was prepared by dissolving Tris powder (Sigma-Aldrich,  $\geq$  99.9 % purity) into Milli-Q water. A 10.0 g aliquot of 0.145 mM mCP stock solution and a 5.0 g aliquot of the 0.2 M Tris stock solution were diluted with 47.0 g Milli-Q water. The pH of these mixed solutions was then adjusted using concentrated HCl (Fisher Scientific, Trace metal grade) according to the temperature-dependent pKa of the Tris buffer  $^{27}$ . Milli-Q water was then added to these buffer solutions to reach a total weight of 50.0 g and to keep the mCP concentration constant. The pH of these Tris buffer solutions was monitored to be close to 8.1 at 25 °C, 7.8 at 35 °C, 7.6 at 45 °C, 7.5 at 50 °C and 75 °C using a pH electrode and a water bath.

For UV-Vis analysis, a 3 mL aliquot of the Tris-based or HCl/NaOH-based pH buffer solution was added to the quartz cuvette to measure the absorbance intensity of the protonated (HI<sup>-</sup>) and depronated (I<sup>2-</sup>) forms of mCP at their maximum absorbance wavelengths. For example, the maximum absorbance wavelengths of HI<sup>-</sup> and I<sup>2-</sup> at 25 °C are 435 and 578 nm, respectively. Wavelength shifts for both spectra were determined at higher temperature by heating the cuvette using a Peltier cell.

#### 2.2.2. Er-bearing mCP-NaOH solutions

The Er hydrolysis constants were determined at 25 °C and near-neutral to alkaline pH using UV-Vis spectrophotometry in a series of Er-bearing mCP-NaOH solutions. These solutions were measured in quartz cuvettes with a constant mCP concentration of 0.03 mM, a NaOH concentration of 0.13 mM, and Er concentrations ranging between 0 and 0.057 mM. The solutions have a low ionic strength (≤0.001 mol/L) over a pH range from ~7 to 9. The experimental solutions were prepared by first diluting a 50.0 g aliquot of the 0.145 mM mCP stock solution with a 43.0 g aliquot of Milli-Q water and a 32.0 g aliquot of 1.0 mM NaOH stock solution. The latter was prepared by titrating 0.100  $\pm$ 0.001 M NaOH (Inorganic Ventures, NIST traceable standards) into Milli-Q water. Experimental solutions with varying initial Er concentrations were then prepared using 5.0 g aliquots of the mixed mCP-NaOH solution and 5.0 g aliquots from a diluted Er chloride stock solution. The latter was prepared by dissolving Er chloride hexahydrate (Sigma-Aldrich, ≥ 99.9 % purity) into 500 g of Milli-O water, and the Er concentrations were determined by ICP-OES. The UV-Vis absorbance spectra at 435 nm and 578 nm were recorded for a total of eight experimental runs with variable Er concentrations to reach pH values from 7.2 to 9.5. The Er-bearing mCP-NaOH solutions with the highest Er concentration (~0.057 mM) display a yellow color controlled by the protonated form of the mCP chromophore without any visible solid suspensions. Based on repeated UV-Vis absorbance measurements of mCP-NaOH with/without Er solutions, the precision of the absorbance measurements for the protonated HI<sup>-</sup> and deprotonated I<sup>2-</sup> forms of mCP at 435 nm and 578 nm, respectively, was better than 0.005 nm.

#### 2.3. Data treatment

#### 2.3.1. mCP optical properties and dissociation

UV-Vis spectrophotometric measurements of the absorbance properties of mCP are based on the following equilibrium reaction:

$$HI^- \leftrightarrow I^{2-} + H^+$$
 (R1)

where HI<sup>-</sup> and I<sup>2-</sup> are the protonated and deprotonated forms of the weak acid indicator mCP. The mCP dissociation constant ( $K^{\circ}_{\text{mCP},T}$ ) at infinite dilution and temperature T (in °C) is described by,

$$K_{\text{mCP,T}}^{\circ} = \frac{[H^{+}][I^{2-}]}{[HI^{-}]} \cdot \frac{\gamma_{H^{+}} \gamma_{I^{2-}}}{\gamma_{HI^{-}}}$$
(1)

where  $[H^+]$ ,  $[I^{2-}]$ , and  $[HI^-]$  are the molar concentrations (in mol/L), and  $\gamma_{H^+}$ ,  $\gamma_{I^{2-}}$ , and  $\gamma_{HI^-}$  are the activity coefficients of the respective species, which are assumed to be unity and at infinite dilution.

Measured UV-Vis absorbance spectra of mCP at maximum wavelength  $(A_{\lambda})$  in a cuvette with path length L (in cm) can be related to the molar concentrations of the I<sup>2-</sup> and HI<sup>-</sup> species and the molar absorbance coefficients  $(\varepsilon_{I^2-\lambda})$  according to Beer-Lambert's law,

$$A_{\lambda} = \left[ \left( \varepsilon_{\mathrm{I}^{2-},\lambda} \cdot \gamma_{\mathrm{I}^{2-}} \cdot \left[ \mathrm{I}^{2-} \right] \right) + \left( \varepsilon_{\mathrm{HI}^{-},\lambda} \cdot \gamma_{\mathrm{HI}^{-}} \cdot \left[ \mathrm{HI}^{-} \right] \right) \right] \cdot \mathrm{L}$$
 (2)

Rearranging Eqs. 1 and 2 yields the following equation:

$$A_{\lambda} = \left[ \varepsilon_{\mathrm{I}^{2-},\lambda} + \left( \varepsilon_{\mathrm{HI}^{-},\lambda} \cdot \frac{[\mathrm{H}^{+}] \gamma_{\mathrm{H}^{+}}}{\mathrm{K}_{\mathrm{mCP.T}}^{\circ}} \right) \right] \cdot \gamma_{\mathrm{I}^{2-}} \cdot [\mathrm{I}^{2-}] \cdot \mathrm{L}$$
(3)

The ratio of absorbance measurement of  $I^{2-}$  and  $HI^{-}$  ( $R = A_{\lambda 2}/A_{\lambda 1}$ ) at their corresponding maximum absorbance wavelengths  $\lambda_2$  and  $\lambda_1$  (in nm) can be converted to pH at given temperature (pH<sub>T</sub>) according to,

$$pH_{T} = -\log e_{2}K_{mCP,T}^{\circ} + \log(\frac{R - e_{1}}{1 - R\frac{e_{3}}{e_{2}}})$$
(4)

where  $e_1$  to  $e_3$  are the ratios of molar absorbance coefficients of  $I^{2-}$  and  $HI^-$  at their maximum absorbance wavelengths  $\lambda_2$  and  $\lambda_1$  with  $e_1 = \frac{\varepsilon_{HI^-,\lambda 2}}{\varepsilon_{HI^-,\lambda 1}}$ ,  $e_2 = \frac{\varepsilon_{I^{2-},\lambda 2}}{\varepsilon_{HI^-,\lambda 1}}$ , and  $e_3 = \frac{\varepsilon_{I^{2-},\lambda 1}}{\varepsilon_{HI^-,\lambda 1}}$ . Increasing temperature from 25 to 75 °C results in a shift of the maximum absorbance wavelength of  $HI^-$  at  $\lambda_1$  from 435 nm to 428 nm whereas the maximum absorbance wavelength of  $I^{2-}$  at  $\lambda_2$  remains constant at 578 nm.

The ratios of  $e_1$  to  $e_3$  can be retrieved by first determining the molar absorbance coefficients of the fully protonated form of mCP (HI<sup>-</sup>) at mildly acidic pH (~4.0) and the fully deprotonated form of mCP (I<sup>2-</sup>) at highly alkaline pH (~12.0). Finally, the term of  $\log K^{\circ}_{\text{mCP,T}}$  in Eq. 4 was solved by conducting a series of experiments with known intermediate pH values using Tris-HCl buffer solutions. Thus, with the experimentally derived parameters (i.e.,  $e_1$ , to  $e_3$ , and  $\log K^{\circ}_{\text{mCP,T}}$  of mCP) at a given temperature, the pH value of an unknown mCP-bearing solution can be determined from Eq. 4 using UV-Vis spectrophotometry.

#### 2.3.2. Derivation of erbium hydrolysis constants

The pH dependent Er hydrolysis results in the stabilization of Er hydroxyl complexes with varying ligand numbers n from 1 to 3 (i.e.,  $Er(OH)_{2^{+}}$ ,  $Er(OH)_{2^{+}}$ ,  $Er(OH)_{3^{0}}$ ), which can be expressed by the following reaction:

$$Er^{-3+} + nH_2O \leftrightarrow Er(OH)_n^{3-n} + nH^+ \tag{R2}$$

The cumulative hydrolysis constants at infinite dilution (\* $\beta_n$ °) are described according to:

$${}^*\beta_n^{\circ} = \frac{[\text{Er}(\text{OH})_n^{3-n}][\text{H}^+]^n}{[\text{Er}^{3+}]} \cdot \frac{\gamma_{\text{Er}(\text{OH})_n^{3-n}}\gamma_{\text{H}^+}^n}{\gamma_{\text{Er}^{3+}}}$$
(5)

where  $[H^+]$ ,  $[Er^{3+}]$ , and  $[Er(OH)_n^{3-n}]$  are the molar concentrations, and  $\gamma_{H^+}$ ,  $\gamma_{Er^{3+}}$ , and  $\gamma_{Er(OH)_n^{3-n}}$  are the activity coefficient of the respective species. The experiments were designed close to infinite dilution with ionic strength  $\leq 0.001$  mol/L, allowing to assume that activity coefficients are equal to unity.

The number of OH<sup>-</sup> ligand bound to the Er hydroxyl complexes or average ligand number  $\vec{n}$  can be related to the sum of all Er hydroxyl species ( $\sum n[Er(OH)_n^{3-n}]$ , with n=1 to 3) and the total dissolved Er concentration ([Er]) according to the following relation:

$$\vec{n} = \frac{\sum n[\text{Er}(\text{OH})_{\text{n}}^{3-\text{n}}]}{[Er]} \tag{6}$$

Refer to the Supplementary Materials for more details about Er and OH<sup>-</sup> ligand mass balance and determination of the average ligand number. Eqs. 5 and 6 are then be combined to retrieve the cumulative Er hydrolysis constants (\* $\beta_n$ °, with n=1 to 3) from the average ligand number,

$$\vec{n} = \frac{(1-\vec{n}) \cdot {}^*\beta_1^{\circ}}{[H^+]} + \frac{(2-\vec{n}) \cdot {}^*\beta_2^{\circ}}{[H^+]^2} + \frac{(3-\vec{n}) \cdot {}^*\beta_3^{\circ}}{[H^+]^3}$$
(7)

For each Er-bearing mCP-NaOH solutions, the molar concentration of H<sup>+</sup> ([H<sup>+</sup>]) was retrieved from UV-Vis pH measurements using the mCP method described above. Eight experimental runs were conducted at 25 °C with a series of solutions containing variable Er concentrations and covering near-neutral to alkaline pH. These experiments permit deriving a complete set of Er hydrolysis constants, which were calculated using Matlab (Version R2023a), and solving Eq. 7 by multiple linear regression with the normal equations expressed by an 8×5 matrix.

#### 3. Results and discussion

#### 3.1. mCP properties between 25 and 75 °C

#### 3.1.1. Optical properties

The results of the UV-Vis spectrophotometric experiments are listed in Table S1 for the determination of the properties of mCP properties at acidic (pH ~4.0) and alkaline (pH ~12.0) pH from 25 to 75 °C. The UV-Vis absorbance spectra are shown in Fig. 1. In acidic solutions (Fig. 1A), mCP exhibits a

strong absorbance at a wavelength close to 435 nm corresponding to its associated form HI<sup>-</sup>, which is consistent with its characteristics reported previously in the literature by Clayton and Byrne <sup>19</sup>. The absorbance intensity of HI<sup>-</sup> decreases from 25 to 75 °C at the maximum absorption wavelength, and is accompanied by a slight blue shift from 435 to 428 nm because of the temperature effect on the pistacking between the mCP molecules and the intramolecular rotation of the individual mCP molecules <sup>28,29</sup>. In alkaline solutions (Fig. 1B), mCP exhibits a strong absorbance at a wavelength of 578 nm, which corresponds to its dissociated form I<sup>2-</sup> and indicates deprotonation of mCP. The absorbance intensity of I<sup>2-</sup> decreases at temperature from 25 to 75 °C and displays a valley at the maximum wavelength of HI<sup>-</sup>.

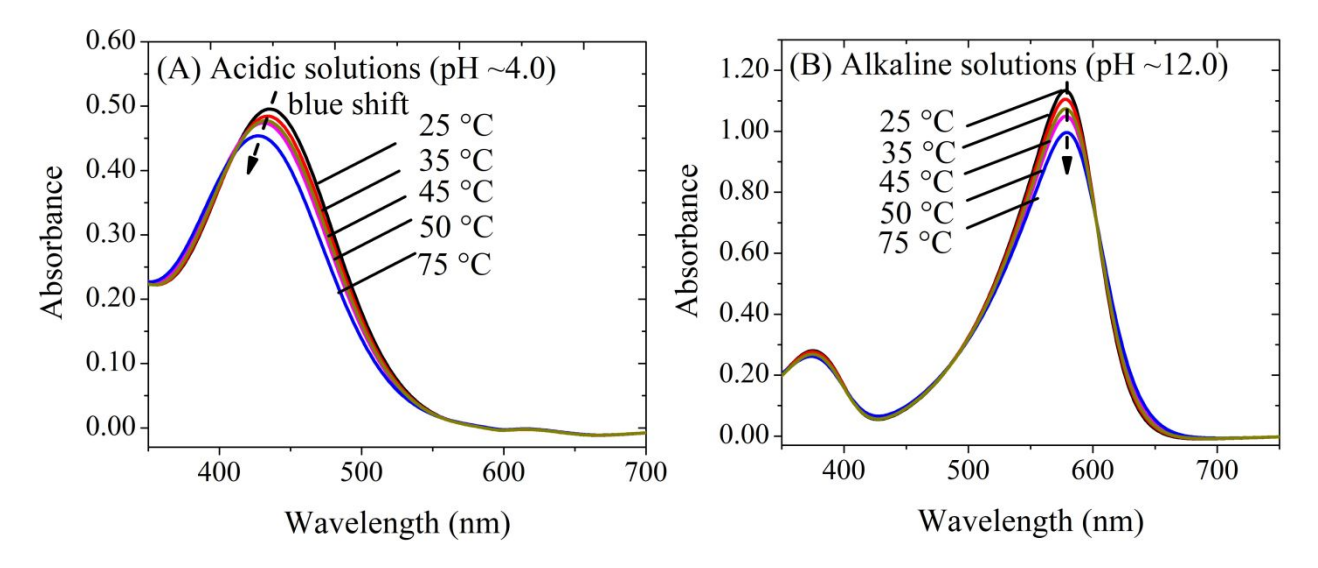


**Figure 1**. (A) UV-Vis absorbance spectra of 0.03 mM mCP solutions at pH of  $\sim$ 4.0 with 0.1 mM HCl at temperatures between 25 and 75 °C. (B) UV-Vis absorbance spectra of 0.03 mM mCP solutions at of pH  $\sim$ 12.0 with 0.01 M NaOH at temperatures between 25 and 75 °C.

#### 3.1.2. Molar absorbance coefficients and dissociation constants

The molar absorbance coefficients of the protonated HI<sup>-</sup> ( $\epsilon_{\text{HI}-\lambda}$ ) and deprotonated I<sup>2-</sup> ( $\epsilon_{\text{I}^2-\lambda}$ ) forms of mCP were calculated from the measured UV-Vis spectra at their maximum absorbance wavelengths (Table S1). The experimental data fit for the temperature dependent molar absorbance coefficients are shown in Fig. 2 and listed in Table 1. At temperatures from 25 to 75 °C, the molar absorbance coefficient of HI<sup>-</sup> decreases systematically at its maximum absorbance wavelength  $\lambda_1$  ( $\epsilon_{\text{HI}-\lambda 1}$ ;  $\lambda_1$  = 435–428 nm), whereas its molar absorbance coefficient at wavelength  $\lambda_2$  ( $\epsilon_{\text{HI}-\lambda 2}$ ;  $\lambda_2$  = 578 nm) shows the opposite trend (Fig. 2A-B). The molar absorbance coefficient of I<sup>2-</sup> decreases also at its maximum absorbance wavelength  $\lambda_2$  ( $\epsilon_{\text{I}^2-\lambda 2}$ ;  $\lambda_2$  = 578 nm), whereas it increases at wavelength  $\lambda_1$  ( $\epsilon_{\text{I}^2-\lambda 1}$ ;  $\lambda_1$  = 435–428 nm) with increased temperature (Fig. 2C-D).

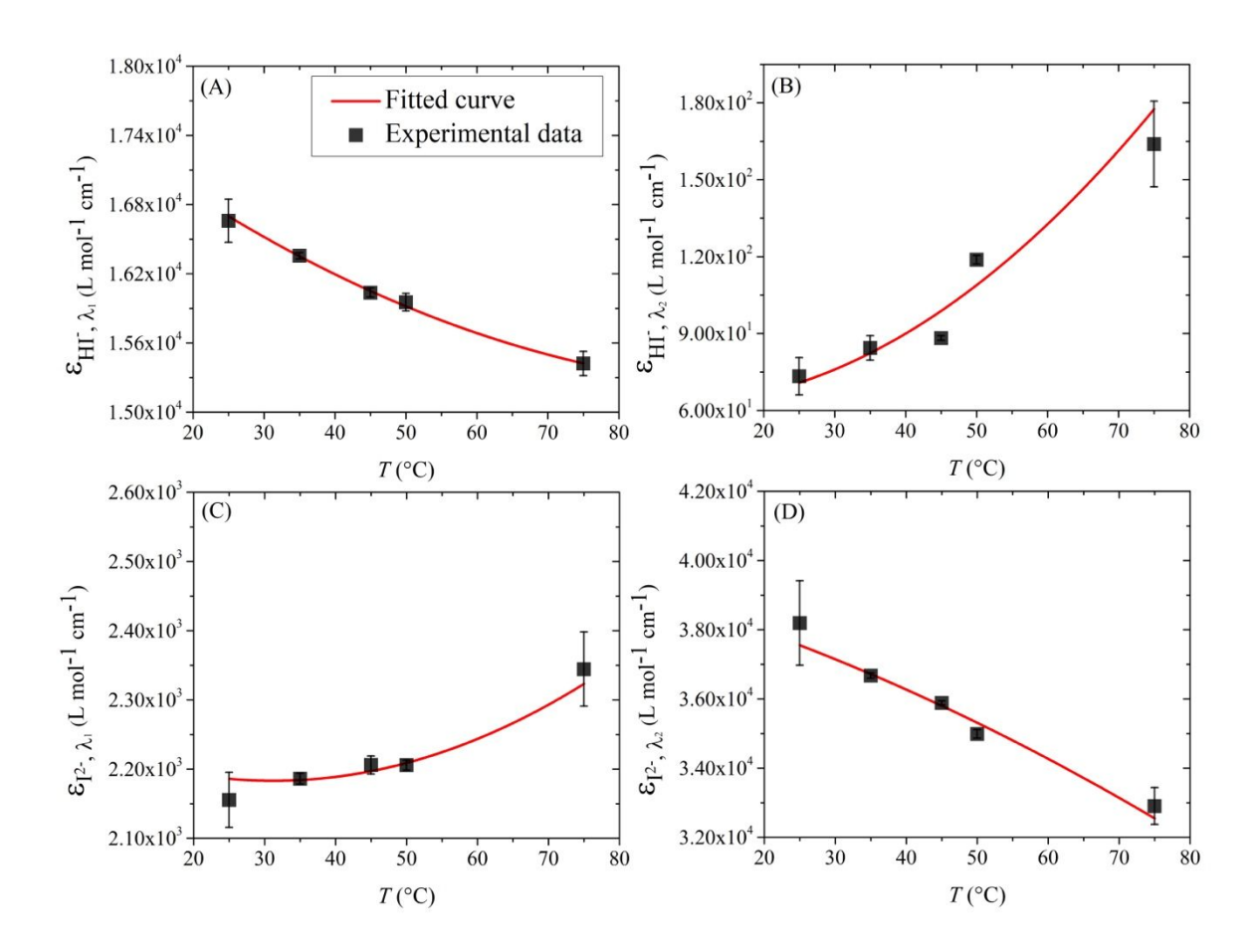


**Figure 2**. (A-B) Temperature dependence of the molar absorbance coefficients of HI<sup>-</sup> at wavelength  $\lambda_1$  (ε<sub>HI- $\lambda_1$ </sub>) and  $\lambda_2$  (ε<sub>HI- $\lambda_2$ </sub>). (C-D) Temperature dependence of the molar absorbance coefficients of I<sup>2-</sup> at wavelengths  $\lambda_1$  (ε<sub>I<sup>2- $\lambda_1$ </sup>) and  $\lambda_2$  (ε<sub>I<sup>2- $\lambda_2$ </sup>). The fitted coefficients of the regressed experimental data are reported in Table 1. The error bars represent the 1σ determined from 3 to 11 replicate experiments.</sub></sub>

**Table 1**. Regressed fits of molar absorbance coefficients of HI<sup>-</sup> and I<sup>2-</sup> at wavelengths  $\lambda_1$  and  $\lambda_2$  as function of temperature between 25 and 75 °C.

Species	Wavelength (nm)	Fitted equation <sup>a</sup>	$\mathbb{R}^2$
HI-	$\lambda_1$ , 435 to 428	$\varepsilon_{\text{HI-},\lambda 1} = 0.1709 \times T^2 - 43.86 \times T + 17600$	0.9986
HI-	$\lambda_2$ , 578	$\varepsilon_{\text{HI}^-,\lambda 2} = 0.0163 \times \text{T}^2 + 0.2215 \times \text{T} + 56.33$	0.9558
$I^{2-}$	$\lambda_1$ , 435 to 428	$\varepsilon_{I^2-,\lambda I} = 0.0555 \times T^2 - 1.9192 \times T + 2175$	0.9852
I <sup>2-</sup>	$\lambda_2$ , 578	$\epsilon_{I^2-,\lambda 2} = 0.6589 \times T^2 - 170.7 \times T + 41997$	0.9937

<sup>&</sup>lt;sup>a</sup>Temperature T is in °C.

The molar absorbance coefficient ratios  $e_1$ ,  $e_2$ , and  $e_3$  need to be evaluated at each temperature from the experimental data in order to determine the pH (Eq. 4) of an unknown solution using the UV-Vis/mCP method. The experimental and fitted values determined in the 0.1 mM HCl and 0.01 M NaOH solutions are shown in Fig. 3 and listed in Table 2. The absorbance coefficient ratios of both

 $e_1$  and  $e_3$  increase between 25 and 75 °C, whereas the absorbance coefficient ratio  $e_2$  decreases in this temperature range. Fits to the experimental data indicate a linear relationship between the absorbance coefficient ratios  $e_1$ ,  $e_2$ , and  $e_3$  and temperature with high R<sup>2</sup> and Pearson correlation coefficient values. The results of  $e_1$ ,  $e_2$ , and  $e_3$  derived from this study are the first data for the mCP absorbance coefficient ratios above to 30 °C at low ionic strength ( $\leq 0.01 \text{ mol/L}$ ). Comparison to literature values indicates agreement on the values of  $e_2$  and  $e_3$  with the study by Lai et al. <sup>18</sup> conduced at 25 and 30 °C whereas  $e_1$  has a larger discrepancy (Table 2).

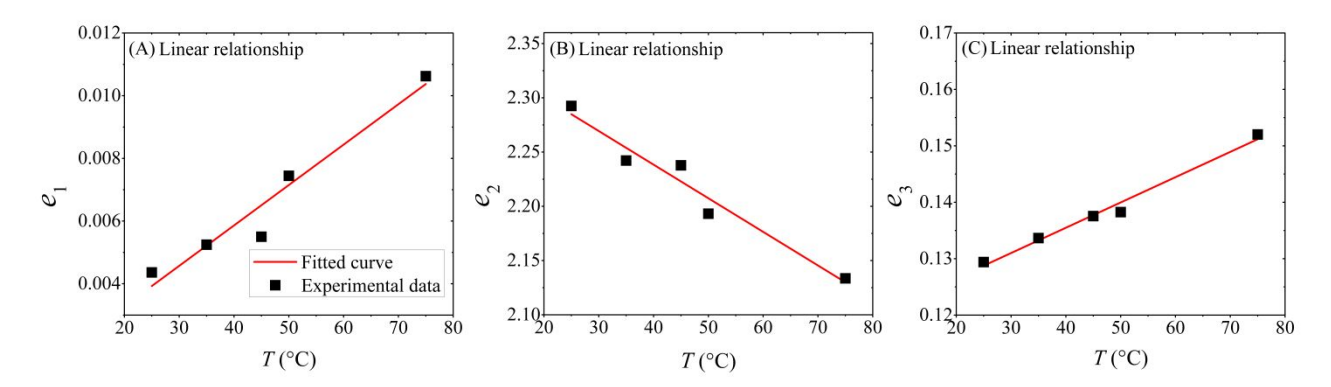


**Figure 3**. Temperature dependence of the molar absorbance coefficient ratio (A)  $e_1$ , (B)  $e_2$ , and (C)  $e_3$  of mCP at temperatures of 25–75 °C. The regressions from the fitted curves are reported in Table 2.

**Table 2**. Molar absorbance coefficient ratios ( $e_1$ - $e_3$ ) and logarithmic value of the dissociation constant of mCP ( $\log K^{\circ}_{\text{mCP,T}}$ ) regressed from the experimental data (Table S1) as a function of temperatures between 25 and 75 °C. Both of the  $e_1$ - $e_3$  and  $\log K^{\circ}_{\text{mCP,T}}$  are used in Eq. 4 to determine the pH value. Also listed is a comparison between values derived in our study at 25 and 30 °C and reported values from Lai et al.<sup>18</sup>.

		$\mathbb{R}^2$	Pearson	Pearson 25		30	30 °C	
Term	Fitted equation <sup>a</sup>		correlation coefficient	This study	Lai el al. (2016)	This study	Lai el al. (2016)	
$e_1$	$e_1 = 1.289 \times 10^{-4} \times T + 7.052 \times 10^{-4}$	0.9280	0.9726	0.03928	0.006019	0.004572	0.006179	
$e_2$	$e_2 = -0.0031 \times T + 2.362$	0.9409	-0.9776	2.285	2.306	2.269	2.298	
$e_3$	$e_3 = 4.483 \times 10^{-6} \times T + 0.1176$	0.9804	0.9926	0.1288	0.1215	0.1310	0.1242	
logK° <sub>mCP,</sub>	$logK^{\circ}_{mCP,T} = -1.853 \times _{T} 10^{-4} \times T^{2} + 2.372 \times 10^{-2} \times T - 9.113$	0.9685	0.7443	-8.64	-8.65	-8.57	-8.61	

<sup>&</sup>lt;sup>a</sup>Temperature T is in °C.

The dissociation constants of mCP ( $K^{\circ}_{mCP,T}$ ) were determined in a series of experiments between 25 and 75 °C by solving Eq. 4 and using the retrieved molar absorbance coefficients as a function of temperature (Table 2). The absorbance spectra of mCP were monitored at each temperature in 0.02 M Tris buffer solutions with known pH values from 7.3 to 8.1 (Table S1). The absorbance peak of HI<sup>-</sup> displays a gradual slight blue shift from 435 nm to 428 nm as well as an increase in absorbance intensity from 25 to 75 °C, whereas the absorbance of I<sup>2-</sup> decreases at its maximum absorbance wavelength of 578 nm (Fig. 4). These results indicate that pH of these mCP-bearing Tris buffer solutions decreases with increasing the temperature from 25 to 75 °C. This trend is consistent with the pH values determined from potentiometric measurements (Table S1).

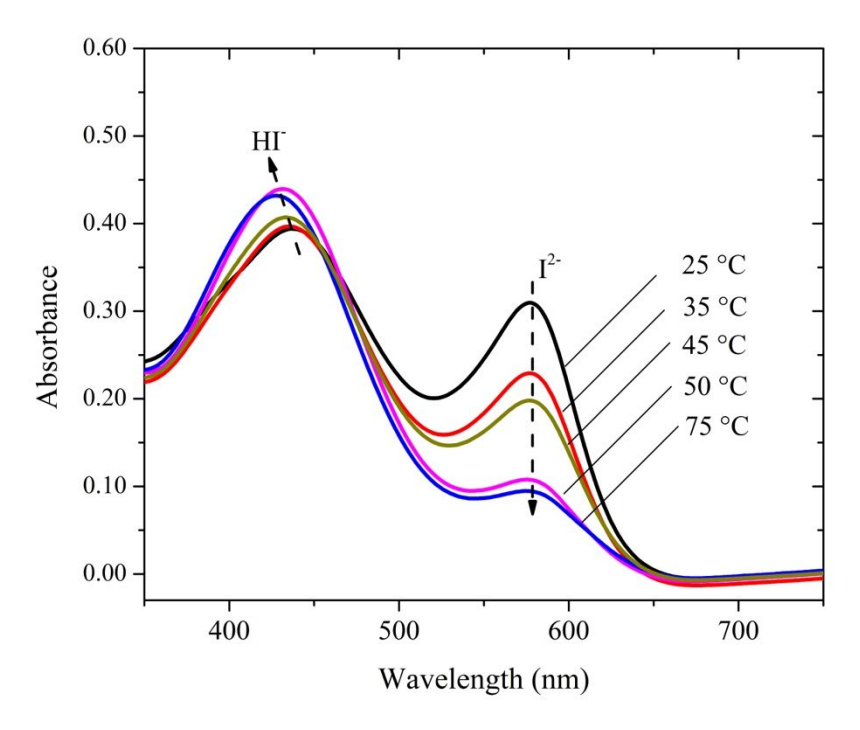


**Figure 4**. UV-Vis spectra of 0.03 mM mCP in 0.02 M Tris-HCl buffer solutions at temperatures between 25 and 75 °C.

The dissociation constants of mCP retrieved as a function of temperature are shown in Fig. 5. The  $\log K^{\circ}_{\text{mCP,T}}$  values increase from -8.64 to -8.38 between 25 and 75 °C and are fitted to a polynomial equation with the coefficients listed in Table 4. The  $\log K^{\circ}_{\text{mCP,T}}$  values of -8.64 and -8.57 at 25 and 30 °C derived from our study are close to the  $\log K^{\circ}_{\text{mCP,T}}$  values of -8.65 and -8.61 reported in the literature by Lai et al.  $^{18}$ . The  $\log K^{\circ}_{\text{mCP,T}}$  values derived in our study from 25 to 75 °C can thus be used to determine solution pH above 30 °C via the combined UV-Vis/mCP method, which was previously limited to temperatures below 30 °C  $^{18}$ . The pH of a solution is determined from Eq. 4 by measuring the absorbance ratios of  $^{12-}$  and  $^{12-}$  are properties ( $^{12-}$  and  $^$ 

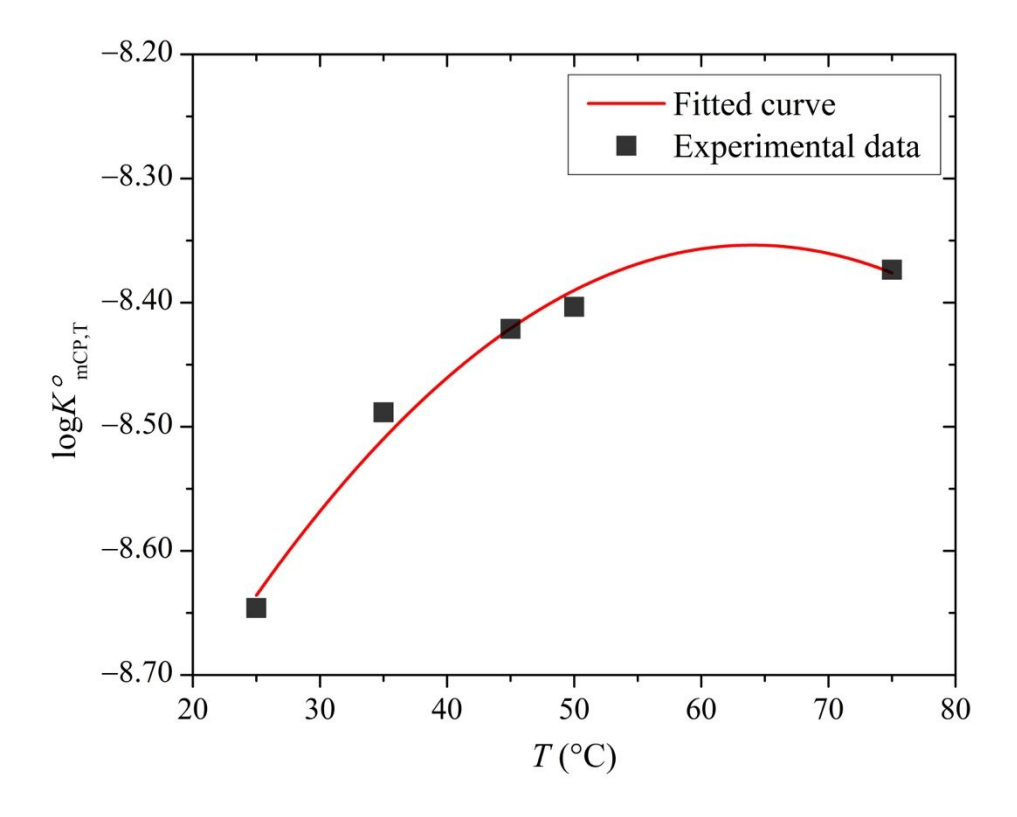


**Figure 5**. Logarithm of the dissociation constant of mCP ( $\log K^{\circ}_{\text{mCP,T}}$ ) determined as a function of temperature. Experimentally derived  $\log K^{\circ}_{\text{mCP,T}}$  data are listed in Table S1, and regressed coefficients for fitted  $\log K^{\circ}_{\text{mCP,T}}$  values are listed in Table 2.

#### 3.2. Erbium hydrolysis at 25 °C

#### 3.2.1. pH determination in Er-bearing solutions

The absorbance intensity of HI<sup>-</sup> and I<sup>2-</sup> were collected on UV-Vis at 25 °C with varying initial Er concentrations ranging from 0 to 0.057 mM (Fig. 6; Table S2). Visual inspection of the Er-bearing mCP-NaOH sample solutions shows that their color gradually changes from purple to yellow with no obvious changes observed at concentrations above 0.04 mM Er. The resulting UV-Vis absorbance spectra (Fig. 6) for these solutions indicate a gradual decrease in intensity at 578 nm (i.e., I<sup>2-</sup> form of mCP) coupled to an increase in absorbance intensity at 435 nm (i.e., HI<sup>-</sup> form of mCP) with an isosbestic point at 488 nm. These results indicate that addition of Er decreases pH from initially alkaline (pH of ~9.5) to near-neutral (pH of ~7.0) due to hydrolysis of Er<sup>3+</sup> ions and deprotonation according to the reaction R2. The measured UV-Vis spectra of mCP are then combined with the optical properties of mCP (Table 4) to retrieve *in situ* pH of the experimental solutions via Eq. 4. The well-defined isosbestic point in the UV-Vis spectra (Fig. 6) suggests that the mCP concentration remains constant and mCP therefore does not have any major influence on the Er hydrolysis in the

experimental solutions. Furthermore, Schwarzenbach and Flaschka mentioned that sulfonphthalein pH indicators like mCP have no ability to form complexes with metal ions <sup>30</sup>.

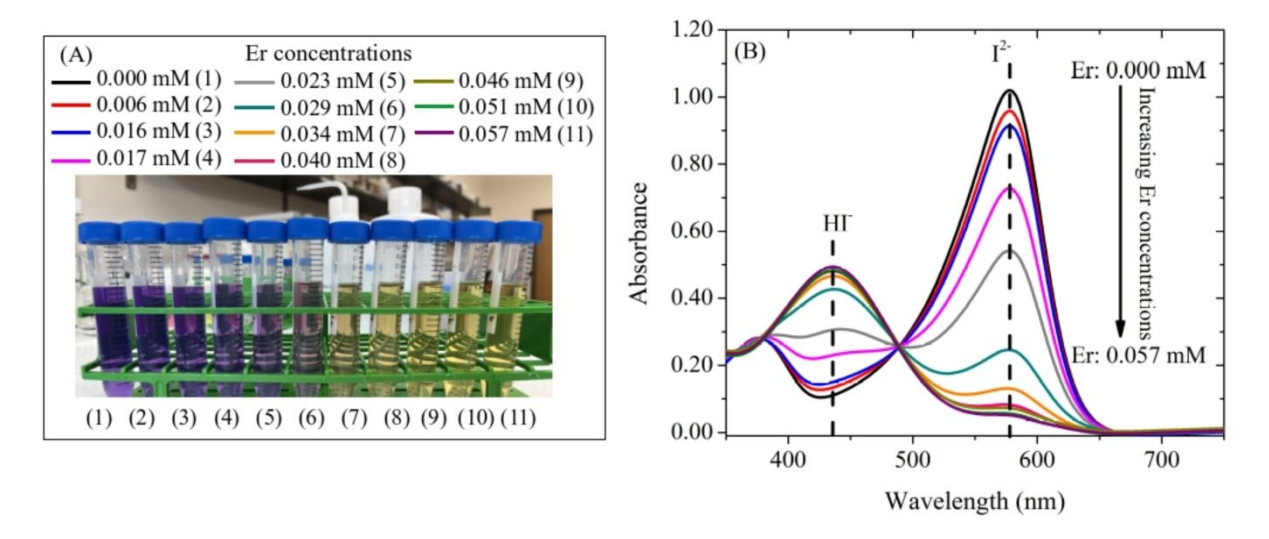


**Figure 6**. (A) Photograph of varying colors from alkaline (left) to near-neutral (right) solutions containing 0.03 mM mCP and 0.13 mM NaOH with varying initial Er concentrations ranging from 0 to 0.057 mM. (B) UV-Vis absorbance spectra of 0.03 mM mCP in 0.13 mM NaOH with addition of varying Er concentrations from 0 mM to 0.057 mM at 25 °C. The compositions of the solutions used in the UV-Vis experiments are listed in Table S2.

The results from the solution color changes also corroborate with a decrease in the mCP absorbance intensity ratio (A<sub>578</sub>/A<sub>435</sub>) at wavelengths of 578 nm (I<sup>2-</sup> form of mCP) and 435 nm (HI-form of mCP). This ratio gradually reaches a minimum with addition of Er concentrations close to 0.057 mM (Fig. 7A). We therefore conclude that UV-Vis spectrophotometric determination of pH for the derivation of the hydrolysis constants of Er using mCP is most reliable between pH values of 7.2 to 9.5 at 25 °C. A comparison between pH determined from UV-Vis spectrophotometry and potentiometric measurements at 25 °C (Fig. 7B) was used to determine the accuracy of pH values retrieved in each Er-bearing sample solutions. A stepwise increase of the initial Er concentrations from 0 to 0.057 mM results in absorbance intensity ratios (A<sub>578</sub>/A<sub>435</sub>) displaying a steep decrease and gradual plateauing at pH below 7.2 (Fig. 7A-B). This effect is due to color oversaturation of the mCP indicator in the solutions containing the highest Er concentrations and resulting in pH discrepancies of >2 % when comparing UV-Vis and potentiometric measurements (Fig. 7C). In contrast, at pH from 7.2 to 9.5, the pH determination by UV-Vis/mCP has a high accuracy with differences <1.5 % in comparison to potentiometric measurements (Fig. 7B). A similar observation was made in the study by Lai et al. <sup>18</sup>, who determined consistent pH result between UV-Vis and potentiometric

measurements in phosphate buffer solutions with pH values ranging from 7.5 to 8.1. A lower accuracy and precision may be present when using unpurified mCP, which results in interference with the absorbance peak of the protonated HI<sup>-</sup> species. Consequently, the smaller mCP absorbance intensity ratio value ( $A_{578}/A_{435}$ ) lowers the derived pH values. Thus, the use of purified mCP such as used in this work is crucial to eliminate any effects on pH measurements using this UV-Vis/mCP method for the determination of the hydrolysis of REE. In addition to the mCP purity and temperature dependence, the accuracy of pH measurement using this combined UV-Vis/mCP method may also depend on the electrolyte and its concentration used in the experiments. DeGrandpre et al. <sup>23</sup> and Lai et al. <sup>18</sup> reported mCP properties ( $e_1$  to  $e_3$  and  $K_{mCP}$ ) that do not display significant differences at ionic strength between 0 and 0.005 mol/L. However, the properties for mCP may need to be corrected for accurate pH measurement in high ionic strength solutions.

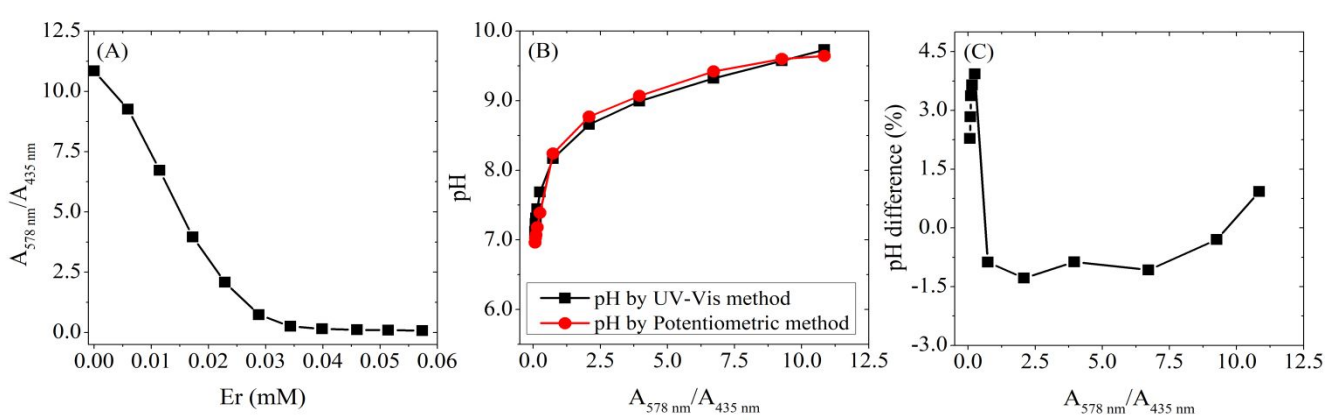


**Figure 7**. (A) Absorbance intensities ratios at 578 nm to 435 nm ( $A_{578}/A_{435}$ ) in the mCP-NaOH solutions with varying initial Er concentrations (0 to 0.057 mM). (B) Comparison of pH values determined from potentiometric and UV-Vis spectrophotometric measurements at 25 °C. (C) Percent pH difference between UV-Vis ( $pH_{UV-Vis}$ ) and potentiometric measurements ( $pH_{pot}$ ) determined by the following equation: ( $[pH_{UV-Vis}-pH_{pot}]/average[pH_{UV-Vis},pH_{pot}]$ ).

#### 3.2.2. Determination of average OH- ligand numbers and hydrolysis constants of Er

The calculated average number of OH<sup>-</sup> ligands bound to Er hydroxyl complexes was determined from the UV-Vis measurements (Supplementary Materials) are shown in Fig. 8 and listed in Table S2. The fitted curve demonstrates a gradual increase of average ligand numbers from ~1.0 to  $2.5 \pm 0.5$  at pH from 7.2 to 9.5 and at 25 °C, suggesting that the Er hydrolysis is dominated by variable proportions of  $Er(OH)^{2+}$ ,  $Er(OH)^{2+}$ , and  $Er(OH)^{30}$  species (Reaction R2, for n=1 to 3). These results are interpreted to indicate that  $Er(OH)^{2+}$  is the predominant species at near-neutral pH and  $Er(OH)^{2+}$  and  $Er(OH)^{30}$  are predominant at more alkaline pH.

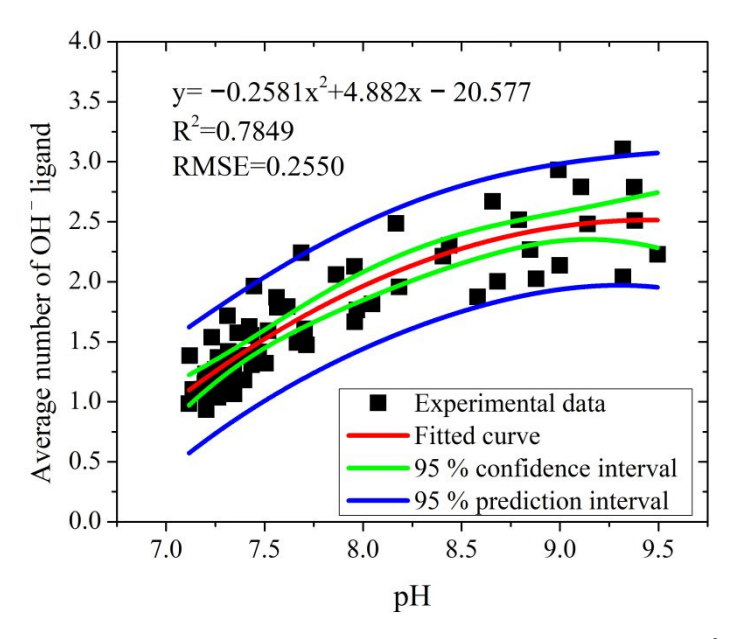


**Figure 8**. Calculated average number of OH<sup>-</sup> ligand coordinated with Er<sup>3+</sup> and pH determined by UV-Vis in experimental mCP-NaOH solutions with varying initial Er concentrations (0 to 0.057 mM Er) and pH values between 7.2 to 9.5. Also shown are the fits to the experimental data, their 95 % confidence and prediction interval, and the fitted coefficients and equation. The experimental data are listed in Table S2.

Comparison of our data with the UV-Vis spectrophotometric data by Stepanchikova et al.  $^{31}$  for the hydrolysis of Tm<sup>3+</sup>, indicates that the average number of OH<sup>-</sup> ligand coordinated to Tm<sup>3+</sup> is similar to Er<sup>3+</sup>. Stepanchikova et al.  $^{31}$  report an average ligand number of  $\sim$ 1.0 at pH of 7.2 to 7.5 and  $\sim$ 2.5 at pH close to 9.5. Their results indicate that Tm(OH)<sup>2+</sup> is the predominant species at nearneutral pH, whereas both Tm(OH)<sub>2</sub><sup>+</sup> and Tm(OH)<sub>3</sub><sup>0</sup> were identified at more alkaline pH. While Stepanchikova et al.  $^{15}$  reports hydrolysis constants for Er<sup>3+</sup>, there are no average ligand numbers reported in that study.

The hydrolysis constants ( $\log^*\beta_n^\circ$ ) of  $Er(OH)^{2^+}$ ,  $Er(OH)_2^+$ , and  $Er(OH)_3^0$  were retrieved from the measured average number of  $OH^-$  ligand and pH according to Eq. 7. To solve this equation, requires a large number of experimental solutions with a wide range of pH values and Er concentrations (Table S2). The retrieved hydrolysis constants at 25 °C are listed in Table 3 and compared to literature values. Based on the average ligand numbers reaching a maximum of ~2.5 to 3 (Fig. 8), we conclude that the  $Er(OH)_4^-$  cannot be identified in our experiments at alkaline pH values up to 9.3. Fig. 9 further shows that our experimental data overlap with the modeled speciation based on the  $\log^*\beta_n^\circ$  values from this study (Table 3). These results indicate that the logarithm Er molality versus pH relationship is controlled by the hydrolysis of Er (R2). In contrast, the formation of colloids

or Er precipitates would result in deviations from the modeled curve in Fig. 9B to lower Er concentrations for given pH value or displaying a change in slope predicted by the equilibrium thermodynamics, which are not observed in these experiments. Fig. 9A also shows that the pH from potentiometric measurements have a wider spread and deviate from both the UV-Vis measurements and the model at pH below of ~8. This can be related to multiple issues while using a pH electrode in an open beaker, stirring of the solution and CO<sub>2</sub>(g) contamination, and longer pH electrode stabilization times. It is noteworthy that potentiometric measurements deviate from the modeled pH for solutions with the highest Er concentrations that are buffered by Er hydrolysis over the NaOH base buffer capacity.

Several other studies  $^{32,33}$  have investigated the solubility of La(OH)<sub>3</sub>(s), Eu(OH)<sub>3</sub>(s), and Am(OH)<sub>3</sub>(s) at 25 °C to discuss the formation of their hydroxyl species at alkaline pH up to 13. The lack of increased REE hydroxide solubility with pH, even at those alkaline pH values, indicates that a higher order REE hydroxyl complex such as Eu(OH)<sub>4</sub><sup>-</sup> is unlikely to be stable. The reviews by Jordan et al. <sup>9</sup> and Guillaumont <sup>34</sup> further only recommend the hydrolysis constants of three hydroxyl species (i.e.,  $\beta_1$  to  $\beta_3$ ) for Eu and Am at 25 °C based on the studies by Berkopf <sup>33</sup> and Silva et al. <sup>35</sup>. These observations are in agreement with a lack of the Er(OH)<sub>4</sub><sup>-</sup> species controlling Er hydrolysis in our experiments (Fig. 9).

**Table 3**. The logarithmic values of the Er hydrolysis constants ( $\log^*\beta_n^\circ$ ,  $Er^{3+} + nH_2O = Er(OH)_n^{3-n} + nH^+$ ) determined in this study at 25 °C using UV-Vis spectrophotometry and mCP over the pH range of 7.2 to 9.5, and comparison to other data at infinite dilution reported in the literature. The standard deviation of the mean ( $1\sigma$ ) is based on multiple UV-Vis experiments for Er-bearing mCP-NaOH solutions with Er concentration ranging between 0 and 0.057 mM (Table S2).

	$^{1}\log^*\beta_n^{\circ}$	1σ	$^{2}\log^{*}\beta_{n}^{\circ}$	$^{3}\log^{*}\beta_{n}^{\circ}$	$^{4}\log^{*}\beta_{n}^{\circ}$	$\frac{5\log^*\beta_n^{\circ}}{}$
n	(This study)			(Klungness and	(Baes and	(Haas et al.)
			et al.)	Byrne)	Mesmer)	
1	-7.22	0.10	-6.73	-7.52	-7.85	-7.76
2	-14.52	0.08	-14.20	-	-15.90	-15.97
3	-23.24	0.04	-24.38	-	-24.20	-24.32

References: ¹This study, spectrophotometry; ²Stepanchikova et al. (2014), spectrophotometry; ³Klungness and Byrne (2000), potentiometry; ⁴Baes and Mesmer (1976), empirical fits and data compilation; ⁵Haas et al. (1995), thermodynamic correlations.

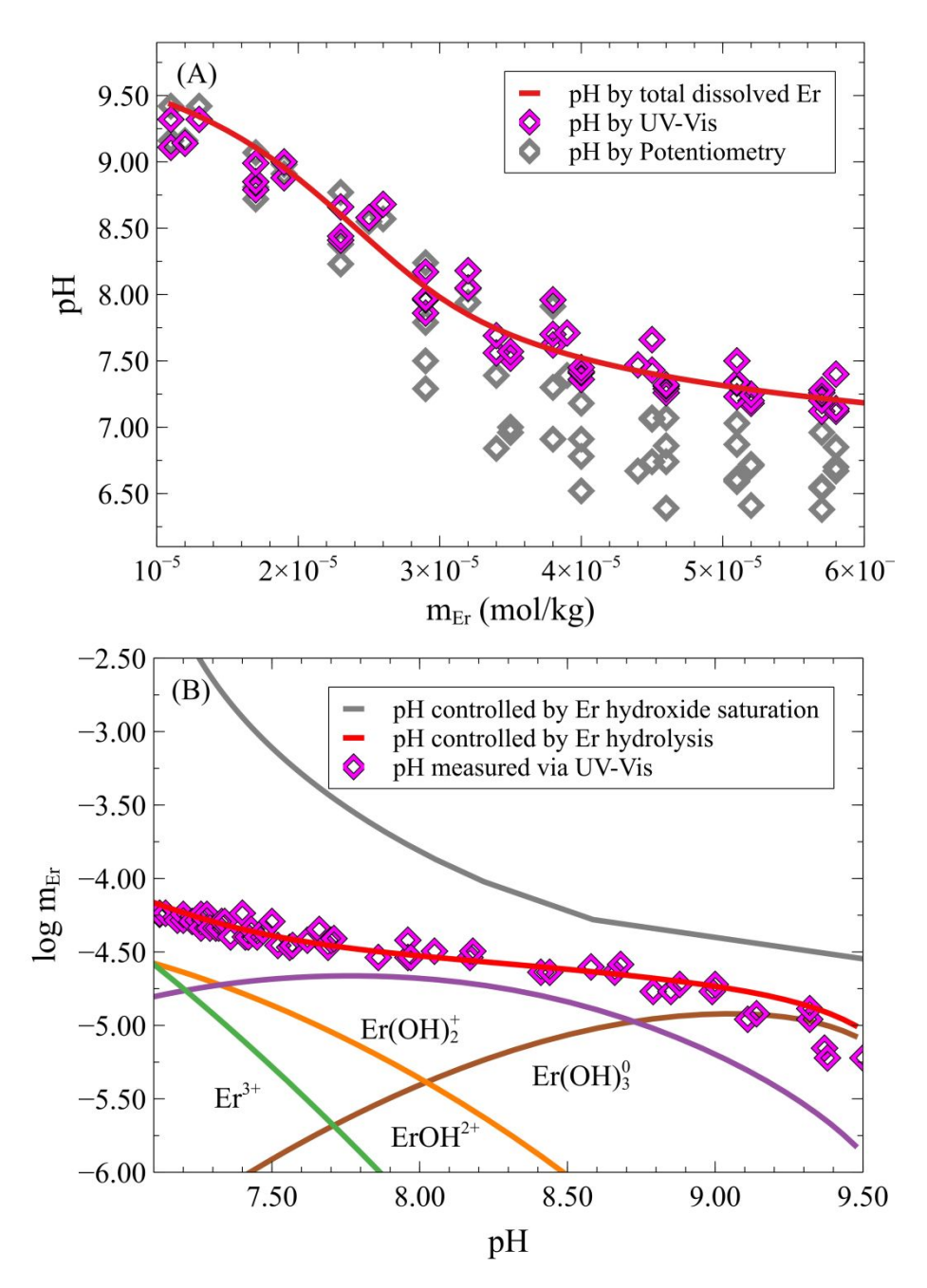


**Figure 9**. Comparison between experimental data and GEMS equilibrium speciation model using the MINES thermodynamic database  $^{36}$  updated with the  $\log^*\beta_n^\circ$  values from Table 3. (A) pH versus total dissolved molality Er (mol/kg) measured using UV-Vis and potentiometry. (B) Total logarithm molality Er versus pH measured via UV-Vis and GEMS models of pH controlled by Er hydrolysis using the  $\log^*\beta_n^\circ$  values from Table 3 and pH controlled by Er hydroxide saturation using the thermodynamic data for Er<sup>3+</sup> from Pan et al.  $^{37}$ , Er(OH)<sub>3</sub>(s) from Diakonov et al.  $^{38}$ , and OH<sup>-</sup> from Shock and Helgeson  $^{39}$ .

The first Er hydrolysis constant  $(\log *\beta_1^\circ)$  for Er(OH)<sup>2+</sup> derived in our study is ~0.3 log units larger that the experimental values determined by Klungness and Byrne using potentiometry (Table

3) <sup>13</sup>. In contrast, the experimental  $\log^*\beta_1^{\circ}$  values by Stepanchikova et al. <sup>15</sup> are ~0.5 log units larger than in our experiments, whereas the values from the compilations of Baes and Mesmer <sup>12</sup> and Haas et al. <sup>40</sup> are both ~0.6 log units smaller. The second Er hydrolysis constant ( $\log *\beta_2^{\circ}$ ) derived in our study is close to the experimental value by Stepanchikova et al. 15, whereas the compilations by Baes and Mesmer <sup>12</sup> and Haas et al. <sup>40</sup> differ by up to 1.4 orders of magnitude. The third Er hydrolysis constant ( $\log^*\beta_3^\circ$ ) derived in our study is about one order of magnitude larger in comparison to the other data by Stepanchikova et al. <sup>15</sup>, Baes and Mesmer <sup>12</sup>, and Haas et al. <sup>40</sup>. The  $\log^*\beta_1^{\circ}$  to  $\log^*\beta_3^{\circ}$ values derived in our study show a close to linear relationship with increased ligand number (Fig. 10A), and both  $\log^*\beta_1^{\circ}$  and  $\log^*\beta_2^{\circ}$  are close to the experimental results by Klungness and Byrne <sup>13</sup> and Stepanchikova et al.15, respectively (Fig 10B). In the most recent publication by Jordan et al.9, the  $\log^*\beta_1^{\circ}$  value for the Eu(OH)<sup>2+</sup> species at 25 °C derived from the study of Klungness and Byrne <sup>13</sup> was recommended. These results provide evidence that the UV-Vis/mCP method is reliable to determine the hydrolysis constants of REE at near-neutral to alkaline solution at 25 °C, and that the data compiled by Baes and Mesmer 12 and Haas et al. 40 need to be revised. Therefore, the UV-Vis/mCP method developed here and also presented by Klungness and Byrne <sup>13</sup> and Stepanchikova et al.15 can now be further applied to the determination of pH and the REE hydrolysis constants up to 75 °C at near-neutral to alkaline pH.

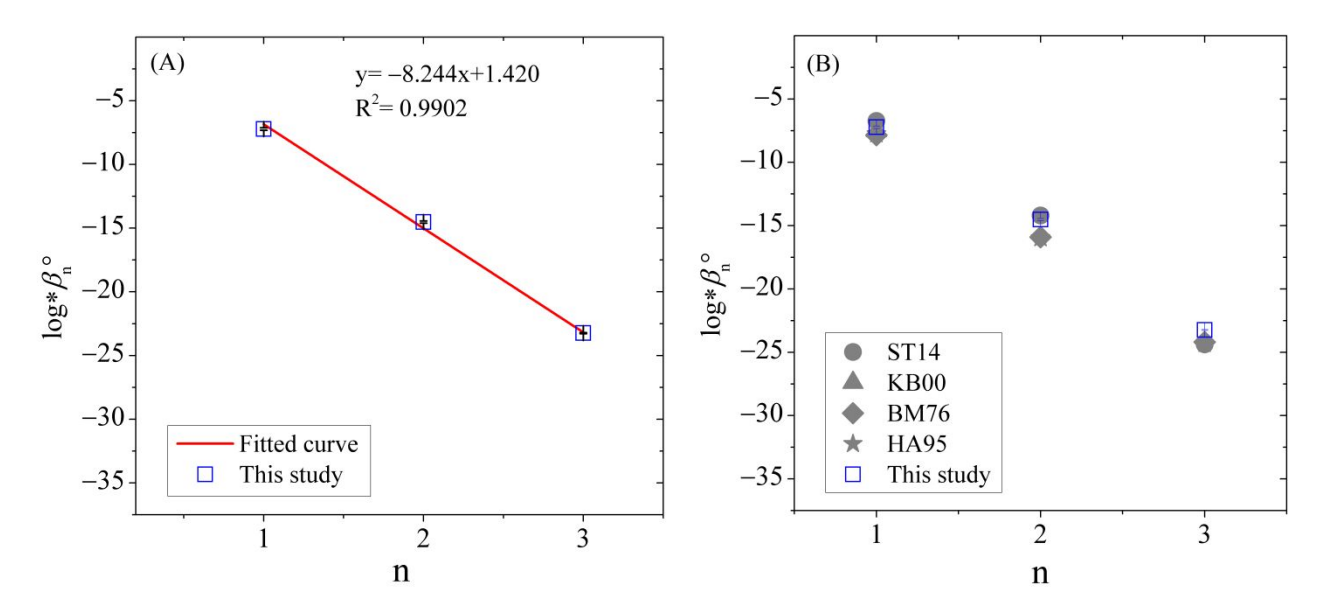


**Figure 10**. (A) Logarithmic values of the hydrolysis constants  $(\log^*\beta_n^\circ)$  of Er  $(Er^{3+} + nH_2O = Er(OH)_n^{3-n} + nH^+$ , with n=1 to 3) at 25 °C derived in this study. (B) Comparison between the  $\log^*\beta_n^\circ$  values derived in this study (Table 3) and literature values. References: [BM76] Baes and Mesmer (1976); [HA95] Haas et al. (1995); [ST14] Stepanchikova et al. (2014); [KB00] Klungness and Byrne (2000).

#### 3.3. Updated Er speciation model at 25 °C and implications for geochemical modeling

Many geochemical modeling programs such as PHREEQC <sup>41</sup> and Geochemist Workbench<sup>® 42</sup> make use of the thermodynamic data for the hydrolysis of REE from the compilation by Baes and Mesmer <sup>12</sup> and the thermodynamic dataset derived by Haas et al. <sup>40</sup>. The latter study is widely used in geochemical modeling databases because it provides the only internally consistent dataset for all of the REE hydroxyl species with extrapolations to elevated temperature. The aqueous species derived by Haas et al. <sup>40</sup> also include other sources of data for the REE aqua ions <sup>40,43</sup>, which are included in the program SUPCRT92 <sup>44</sup> and are collectively referred to here as the Supcrt92 database.

The speciation of Er was calculated at 25 °C as a function of pH using the new hydrolysis constants derived in this study (Table 3) and compared to predictions using the data from the Supcrt92 database (Fig. 11). At pH below 7.2, Er<sup>3+</sup> is the major species in both models, but our study displays a significantly higher Er hydroxyl species stability with a switchover at pH of  $\sim$ 7.2 with both Er(OH)<sup>2+</sup> and Er(OH)<sub>2</sub><sup>+</sup> species becoming predominant. This contrasts with the speciation model using the Supert92 database, which predicts that the Er hydroxyl complexes start only to predominate at a pH above 7.8. Speciation calculations based on our experimental data further indicate a large predominance field of Er(OH)<sub>2</sub><sup>+</sup> over a pH range of 7.5 to 8.7, with a switchover to Er(OH)<sub>3</sub><sup>0</sup> at a pH of ~8.7. In contrast, speciation calculations using the data from Supert92 predict a narrower predominance field for all three Er hydroxyl complexes Er(OH)<sup>2+</sup>, Er(OH)<sub>2</sub><sup>+</sup>, and Er(OH)<sub>3</sub><sup>0</sup> species at pH below ~8.5. The hydrolysis constants from Baes and Mesmer <sup>12</sup> are very close to those from the Supert92 database (Table 3), thus resulting in a similar modeled speciation. Therefore, we recommend updating the REE hydrolysis constant provided from the Supert92 database and from Baes and Mesmer <sup>12</sup> compilation because these will result in considerable under predictions of the stability of REEOH<sub>2</sub><sup>+</sup> and REE(OH)<sub>3</sub><sup>0</sup> hydroxyl complexes as illustrated in Fig. 11. Hence, there is an urgent need to revise the thermodynamic data for the REE hydroxyl complexes to accurately model the speciation of REE in natural waters.

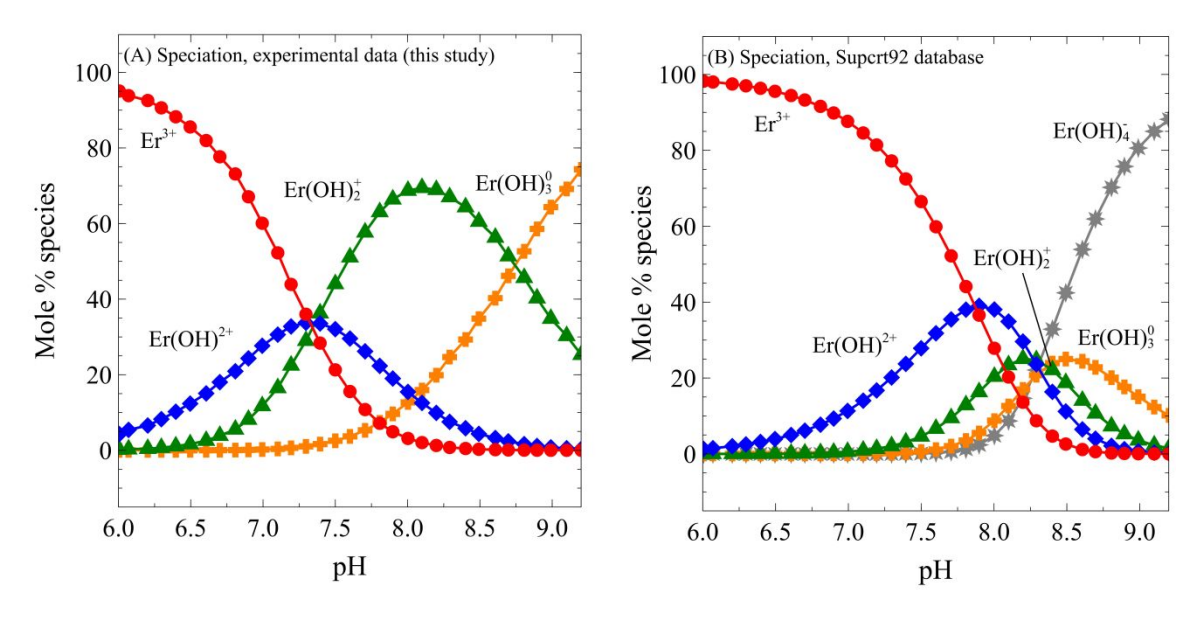


**Figure 11**. Speciation distribution diagrams of Er with pH ranging between 6 to 9.2 at 25 °C. Diagrams were calculated using GEMS code package <sup>45</sup> and a HCl/NaOH titration model using the thermodynamic properties for Er species based on (A) experimental data derived in this study and (B) predictions from the Supert92 database. Thermodynamic properties for other species were taken from the MINES thermodynamic database <sup>36</sup>.

#### 4. Implication to heavy REE mobilization in regolith-hosted ion adsorption deposits

The updated Er hydrolysis constants determined in this study suggest that REE hydroxyl complexes can potentially play a crucial role in the fractionation of light vs. heavy REE in low temperature critical mineral deposits. In order to evaluate this hypothesis, we simulate the mobility of Er at 25 °C in natural water compositions from the Zudong deposit in South China <sup>6</sup>, which is one of the world's largest produced heavy REE regolith-hosed ion adsorption deposit. The pH of the aquifer groundwater for this deposit is around 8.5 and its element composition is available from the study by Li et al. <sup>8</sup>. The groundwater contains the following ligands which can form important REE species: HCO<sub>3</sub><sup>-</sup>, CO<sub>3</sub><sup>2-</sup>, SO<sub>4</sub><sup>2-</sup>, Cl<sup>-</sup>, and F<sup>-</sup>. The geochemical model was performed using the GEMS code package <sup>43</sup> and the thermodynamic properties of Er hydroxyl complexes determined in our experiments, and for comparison the predicted values from the Supcrt92 database. Thermodynamic properties of aqueous species, gases, and minerals involving in the geochemical modeling of the Zudong deposit groundwater were taken from the MINES thermodynamic database <sup>36</sup>. The sources for the thermodynamic properties of all other Er aqueous species are listed in Table S3.

The simulated Er speciation in the Zudong deposit aquifer groundwater is shown as a function of pH in Fig. 12. The Er<sup>3+</sup> aqua ion and the Er fluoride, sulfate, chloride, and fluoride become replaced by the Er carbonate complexes from acid to near-neutral. While the latter dominates in a wide pH

range, an increase from near-neutral to alkaline pH results in an increased competition between the Er hydroxyl and carbonate complexes in both geochemical models. Li et al.  $^6$  proposes that the anomalously high proportion of heavy REE in clay-sorbed fraction of this deposit is attributed to the sorption of positively charged carbonate complexes on the negatively charged surfaces of clay minerals (e.g. kaolinite) during weathering and the interaction of the regolith with groundwater. The heavy REE are released from the primary REE minerals bedrock like synchysite-(Y) and then combined with ligands such as  $HCO_3^-$  and  $CO_3^{2-}$  to be transported as charged aqueous complexes (i.e.,  $REECO_3^+$  or  $REE(HCO_3)^{2+}$ ).

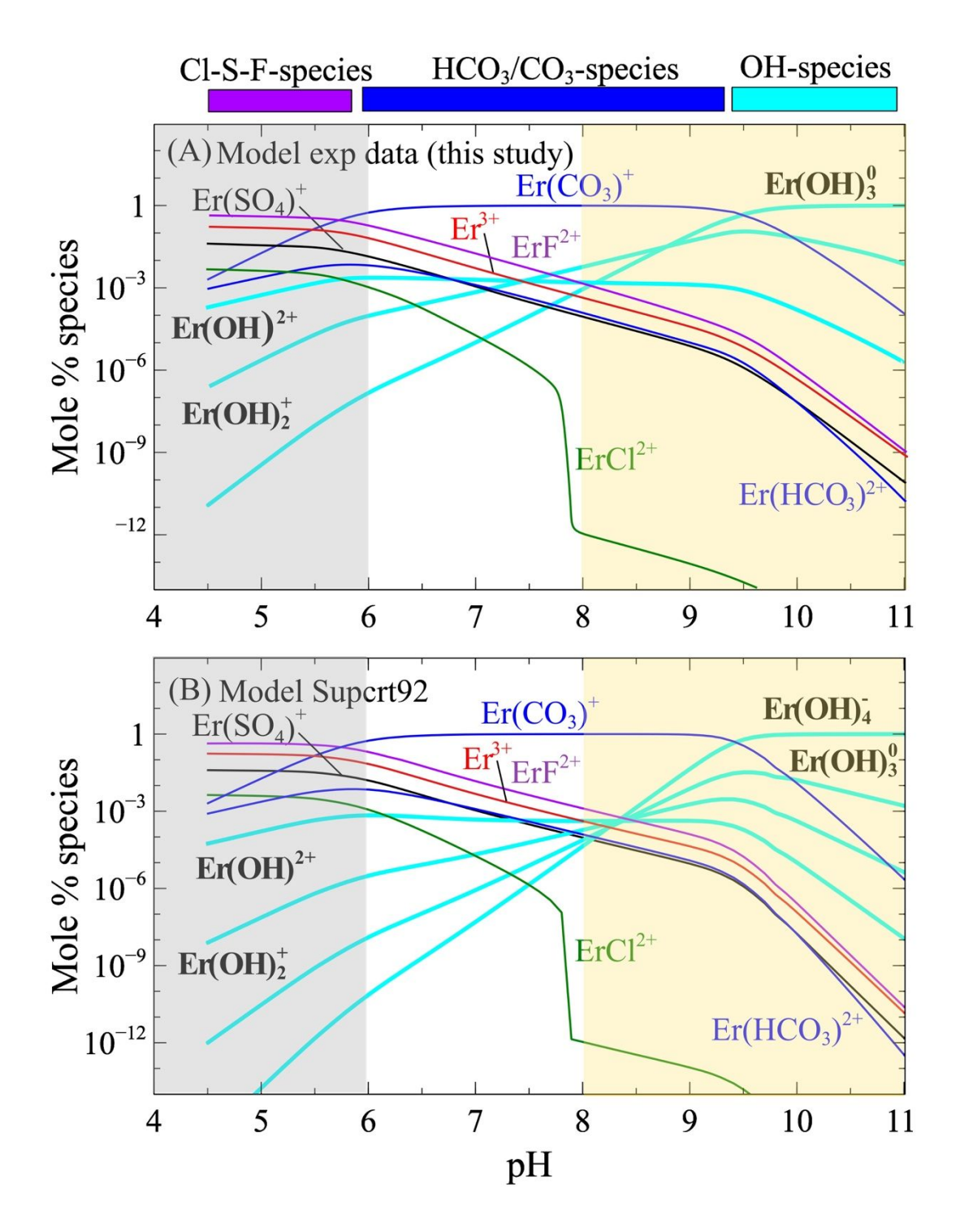


**Figure 12**. Geochemical model of Er speciation as a function of pH calculated at 25 °C using the GEMS code package and the aquifer groundwater of the Zudong heavy REE deposit described in the study by Li et al. <sup>8</sup>. A comparison between predictions using (A) the updated hydrolysis constants derived in this study and (B) the Supert92 database indicates an increased importance of the Er(OH)<sub>2</sub><sup>+</sup> species in the updated model (mildly acidic condition in gray shade and alkaline condition in yellow shade). Thermodynamic properties for REE and other species were taken from the MINES thermodynamic database <sup>36</sup>.

Recent experiments by Borst et al. suggest that the REE hydroxyl complexes can also easily adsorb onto clay minerals with an increase in pH to alkaline values <sup>46</sup>. Indeed, the updated geochemical model (Fig. 12A) shows that the Er(OH)<sub>2</sub>+ species increasingly predominate at pH of 7.5 to 9.0 followed by the Er(OH)<sub>3</sub>0 species which gradually dominate in more alkaline aqueous solutions. Thus, another possible explanation for the anomalously high proportion of heavy REE in clay-sorbed fraction of Zudong deposit is that the charged Er(OH)<sub>2</sub>+ species also contributes to the mobilizations and adsorption of REE during regolith-groundwater interaction. The modeling results reinforce the importance of accurate experimentally derived thermodynamic properties for the REE aqueous species to delineate the controlling fluid-rock interaction processes that form these deposits in natural systems. Other potential applications of predictive REE speciation modeling include improvements in the chemical separation and extraction technologies, the synthesis of REE-bearing phases, as well as extraction from new sources such as thermal waters and acid mine drainage.

#### **5.** Conclusions

This work demonstrates a combined UV-Vis/mCP spectrophotometry method to determine the hydrolysis constants of Er hydroxyl complexes at 25 °C and at near-neutral to alkaline pH. We investigated the optical properties of mCP which permits deriving a new set of dissociation constants as a function of temperature up to 75 °C. Comparison of the measured pH by potentiometric method and pH determined by the UV-Vis/mCP method indicates a close agreement at pH ranging between 7.2 to 9.5. Therefore, the UV-Vis/mCP method developed here can now be further applied to the determination of pH and the REE hydrolysis constants up to to 75 °C at near neutral to alkaline pH. The major species at those conditions were found to be Er(OH)<sup>2+</sup>, Er(OH)<sup>2+</sup>, and Er(OH)<sup>30</sup> at 25 °C, in contrast with predictions based on the Supert92 database or the dataset derived by Haas et al. that significantly underpredict the stability of the Er(OH)<sup>2+</sup> and Er(OH)<sup>30</sup> species. Therefore, there is an urgent need for revising the thermodynamic properties of REE aqueous complexes implemented in popular geochemical modeling programs, even at ambient temperature. These thermodynamic data are needed to accurately simulate the behavior of the REE in natural systems.

#### **Author contribution**

Hannah Juan Han: Writing – original draft, Methodology, Formal analysis, Investigation, Conceptualization, Data curation. Alexander Gysi: Writing – review & editing, Validation, Supervision, Resources, Funding acquisition, Data curation, Conceptualization.

#### **Conflict of interest**

There are no conflicts to declare.

#### Data availability

The data published in this contribution are available as ESI submitted with the manuscript.

#### Acknowledgments

This research is based upon work supported by the U.S. Department of Energy, Office of Science, Office of Basic Energy Sciences, Geosciences program under Award Number DE-SC0021106 to AG. The authors acknowledge the use of the ICP-OES in the analytical chemistry laboratory at New Mexico Bureau of Geology. The authors also thank Bonnie Frey and Dustin Baca for assistance with ICP-OES operation and maintenance.

#### **Supplementary Materials**

Details for all the UV-Vis spectrophotometric experimental data showing the properties of mCP as a function of temperature and hydrolysis constants of Er at 25 °C and sources of thermodynamic data from the Supert92 dataset considered in the Er aqueous speciation modeling for the aquifer groundwater of the Zudong heavy REE deposit are provided in the Supplementary Materials files.

#### References

- 1. S. Cotton, in *Lanthanide and Actinide Chemistry*, John Wiley & Sons, Ltd, England, First edition, 2006, pp. 61–87.
- 2. A. Tukker, Environ. Sci. Technol., 2014, 48, 9973–9974.
- 3. V. Balaram, Geosci. Front., 2019, 10, 1285–1303.
- 4. M. K. Hossain, M. I. Khan and A. El-Denglawey, Appl. Mater. Today, 2021, 24, 101104.
- 5. S. R. Golroudbary, I. Makarava, A. Kraslawski and E. Repo, *Sci. Total Environ.*, 2022, **832**, 155022.
- 6. M. Y. H. Li, M. F. Zhou and A. E. Williams-Jones, *Econ. Geol.*, 2019, **114**, 541–568.
- 7. M. Y. H. Li, M. F. Zhou and A. E. Williams-Jones, *Econ. Geol.*, 2020, **115**, 1097–1118.
- 8. M. Y. H. Li, H. T. Kwong, A. E. Williams-Jones and M. F. Zhou, *Geochim. Cosmochim. Acta*, 2022, **330**, 258–277.

- 9. N. Jordan, T. Thoenen, K. Spahiu, J. Kelling, S. Starke and V. Brendler, *Coord. Chem. Rev.*, 2024, **510**, 215702.
- 10. J. Schijf and R. H. Byrne, *Chem. Geol.*, 2021, **584**, 120479.
- 11. L. C. S. Nascimento, M. L. Torem, E. C. Giese, A. G. Merma, L. C. Bertolino and N. O. A. Anjos, *Miner. Eng.*, 2023, **195**, 108029.
- 12. C. F. Baes and R. E. Mesmer, *The hydrolysis of cations*, Wiley, New York, 1976.
- 13. G. D. Klungness and R. H. Byrne, *Polyhedron*, 2000, **19**, 99–107.
- 14. Y. Y. Yakubovich and V. G. Alekseev, Russ. J. Inorg. Chem., 2012, 57, 911–915.
- 15. S. A. Stepanchikova, R. P. Biteikina, G. P. Shironosova and G. R. Kolonin, *Russ. Geol. Geophys.*, 2014, **55**, 941–944.
- 16. X. Liu, M. C. Patsavas and R. H. Byrne, *Environ. Sci. Technol.*, 2011, 45, 4862–4868.
- 17. R. A. Easley and R. H. Byrne, *Environ. Sci. Technol.*, 2012, **46**, 5018–5024.
- 18. C. Z. Lai, M. D. DeGrandpre, B. D. Wasser, T. A. Brandon, D. S. Clucas, E. J. Jaqueth, Z. D. Benson, C. M. Beatty and R. S. Spaulding, *Limnol. Oceanogr. Methods*, 2016, **14**, 864–873.
- 19. T. D. Clayton and R. H. Byrne, *Deep-Sea Res. Part I*, 1993, **40**, 2115–2129.
- 20. M. P. Seidel, M. D. DeGrandpre and A. G. Dickson, Mar. Chem., 2008, 109, 18–28.
- 21. S. Loucaides, V. M. C. Rèrolle, S. Papadimitriou, H. Kennedy, M. C. Mowlem, A. G. Dickson, M. Gledhill and E. P. Achterberg, *Sci. Rep.*, 2017, 7, 1–11.
- 22. J. D. Müller and G. Rehder, *Front. Mar. Sci.*, 2018, **5**, 1–9.
- 23. M. D. DeGrandpre, R. S. Spaulding, J. O. Newton, E. J. Jaqueth, S. E. Hamblock, A. A. Umansky and K. E. Harris, *Limnol. Oceanogr. Methods*, 2014, **12**, 830–839.
- 24. A. G. Dickson, *Deep Sea Res. Part Oceanogr. Res. Pap.*, 1993, **40**, 107–118.
- 25. R. W. Ramette, C. H. Culberson and R. G. Bates, Anal. Chem., 1977, 49, 867–870.
- 26. T. A. DelValls and A. G. Dickson, *Deep Sea Res. Part Oceanogr. Res. Pap.*, 1998, **45**, 1541–1554.
- 27. N. E. Good, G. D. Winget, W. Winter, T. N. Connolly, S. Izawa and R. M. M. Singh, *Biochemistry*, 1966, 5, 467–477.
- 28. S. A. Stepanchikova and G. I. Galay, Russ. J. Phys. Chem. A, 2017, 91, 73–78.

- 29. A. Pietropaolo, C. Cozza, Z. Zhang and T. Nakano, Liq. Cryst., 2018, 45, 2048–2053.
- 30. G. Schwarzenbach and H. Flaschka, *Complexometric Titrations*, Methuen and Co., London, second edition, 1969.
- 31. S. A. Stepanchikova, R. P. Biteykina and A. A. Sava, Open J. Inorg. Chem., 2013, 03, 42-47.
- 32. Md. Moniruzzaman, T. Kobayashi and T. Sasaki, J. Nucl. Radiochem. Sci., 2020, 20, 32-42.
- 33. M.F. Bernkopf, Hydrolysereaktionen und Karbonatkomplexierung von dreiwertigem Americium im natürlichen aquatischen System, Institut für Radiochemie, Technische Universität München,1984.
- 34. R. Guillaumont, T. Fanghänel, J. Fuger, I. Grenthe, V. Neck, D.A. Palmer, M. H. Rand, Update on the chemical thermodynamics of uranium, neptunium, plutonium, americium and technetium, Elsevier, Amsterdam, 2003.
- 35. R. J. Silva, G. Bidoglio, M. H. Rand, P. Robouch, H. Wanner and I. Puigdomènech, in *Chemical Thermodynamics*, North Holland Elsevier Science Publishers B. V., Amsterdam, Netherlands, Organisation for Economic Cooperation, Development, Ed., 1995.
- 36. A. P. Gysi, N. C. Hurtig, R. Pan, G. D. Miron and D. A. Kulik, MINES Thermodynamic Database, https://geoinfo.nmt.edu/mines-tdb/, (accessed May 21, 2024).
- 37. R. Pan, A. P. Gysi, G. D. Miron and C. Zhu, Chem. Geol., 2024, 643, 121817.
- 38. I. I. Diakonov, K. V. Ragnarsdottir and B. R. Tagirov, Chem. Geol., 1998, 151, 327–347.
- 39. E. L. Shock and H. C. Helgeson, Geochim. Cosmochim. Acta, 1989, 52, 2009–2036.
- 40. J. R. Haas, E. L. Shock and D. C. Sassani, Geochim. Cosmochim. Acta, 1995, 59, 4329–4350.
- 41. D. L. Parkhurst and C. A. J. Appelo, Description of Input and Examples for PHREEQC Version 3—A Computer Program for Speciation, Batch-Reaction, One-Dimensional Transport, and Inverse Geochemical Calculations: U.S. Geological Survey Techniques and Methods, 2013.
- 42. C. M. Bethke, The Geochemist's Workbench Version 4.0: A Users Guide. University of Illinois. Urbana, IL. 2002.
- 43. E. L. Shock, D. C. Sassani, M. Willis and D. A. Sverjensky, *Geochim. Cosmochim. Acta*, 1997, **61**, 907–950.
- 44. J. W. Johnson, E. H. Oelkers and H. C. Helgeson, Comput. Geosci., 1992, 18, 899–947.
- 45. D. A. Kulik, T. Wagner, S. V. Dmytrieva, G. Kosakowski, F. F. Hingerl, K. V. Chudnenko and U. R. Berner, *Comput. Geosci.*, 2013, **17**, 1–24.

46. A. M. Borst, M. P. Smith, A. A. Finch, G. Estrade, C. Villanova-de-Benavent, P. Nason, E. Marquis, N. J. Horsburgh, K. M. Goodenough, C. Xu, J. Kynický and K. Geraki, *Nat. Commun.*, 2020, **11**, 4386.

#### Data availability

The data published in this contribution are available as ESI submitted with the manuscript.